Journal of Controlled Release 334 (2021) 1–10

Contents lists available at ScienceDirect

Journal of Controlled Release

journal homepage: www.elsevier.com/locate/jconrel

Morphologic design of sugar-based polymer nanoparticles for delivery of antidiabetic peptides

Mahmoud Elsabahy [a,b,**], Yue Song [a], Noura G. Eissa [c], Sarosh Khan [a], Mostafa A. Hamad [d], Karen L. Wooley [a,*]

[a] Departments of Chemistry, Chemical Engineering, and Materials Science & Engineering, Texas A&M University, College Station, TX 77842, USA
[b] Science Academy, Badr University in Cairo (BUC), Badr City, Cairo 11829, Egypt
[c] Department of Pharmaceutics and Industrial Pharmacy, Faculty of Pharmacy, Zagazig University, Zagazig 44519, Egypt
[d] Department of Surgery, Faculty of Medicine, Assiut University, Assiut 71515, Egypt

ARTICLE INFO

Keywords:
Nanoparticles
Insulin
Insulin glargine
Spherical
Cylindrical
Platelet

ABSTRACT

Zwitterionic polymer nanoparticles of diverse morphologies (spherical, cylindrical, and platelet-like) constructed from biocompatible sugar-based polymers are designed to extend the pharmacological activities of short- and long-acting insulin peptides, thereby providing potential for therapeutic systems capable of reducing the frequency of administration and improving patient compliance. Amphiphilic block copolymers composed of zwitterionic poly(D-glucose carbonate) and semicrystalline polylactide segments were synthesized, and the respective block length ratios were tuned to allow formation of nanoscopic assemblies having different morphologies. Insulin-loaded nanoparticles had similar sizes and morphologies to the unloaded nanoparticle counterparts. Laser scanning confocal microscopy imaging of three-dimensional spheroids of vascular smooth muscle cells and fibroblasts after treatment with LIVE/DEAD® stain and FITC-insulin-loaded nanoparticles demonstrated high biocompatibility for the nanoconstructs of the various morphologies and significant intracellular uptake of insulin in both cell lines, respectively. Binding of short-acting insulin and long-acting insulin glargine to nanoparticles resulted in extended hypoglycemic activities in rat models of diabetes. Following subcutaneous injection in diabetic rats, insulin- and insulin glargine-loaded nanoparticles of diverse morphologies had demonstrated up to 2.6-fold and 1.7-fold increase in pharmacological availability, in comparison to free insulin and insulin glargine, respectively. All together, the negligible cytotoxicity, immunotoxicity, and minimal cytokine adsorption onto nanoparticles (as have been demonstrated in our previous studies) provide exciting and promising evidence of biocompatible nanoconstructs that are poised for further development toward the management of diabetes.

1. Introduction

Reducing the frequency of dosing and, subsequently, the amount of carrier and excipients used to deliver active pharmaceutical ingredients could improve patient compliance, particularly for elderly patients, children and in certain diseases and conditions, and reduce the toxicity associated with the frequent administration of formulations in which the drug is encapsulated [1]. Several biomolecules, for instance, peptides, are sensitive to the harsh environment in the gastrointestinal tract and have insufficient permeability through the intestinal mucosa, due to their high molar mass and hydrophilicity [2]. Subcutaneous delivery of peptides is considered an effective and well-tolerated route of administration. However, subcutaneous administration is associated with a lack of patient compliance, stress from daily injection, and risk of infection. Hence, there remains a need for drug delivery platforms that provide prolonged bioactivity of biomolecules following subcutaneous administration [3].

A prolonged delivery platform is designed to extend antidiabetic peptide release time and stability, increase bioavailability, and maximize therapeutic efficacy, and, importantly, improve patient compliance

* Corresponding author.
** Corresponding author at: Departments of Chemistry, Chemical Engineering, and Materials Science & Engineering, Texas A&M University, College Station, TX 77842, USA.
E-mail addresses: mahmoud.elsabahy@buc.edu.eg (M. Elsabahy), wooley@chem.tamu.edu (K.L. Wooley).

https://doi.org/10.1016/j.jconrel.2021.04.006
Received 3 March 2021; Received in revised form 5 April 2021; Accepted 8 April 2021
Available online 18 April 2021

via reducing the frequency of administration. Diabetes has been selected as a model disease, due to the dramatic rise in diabetes prevalence, which is estimated to rise from 425 million adults in 2017 to 629 million by 2045, according to the International Diabetes Federation (www.idf.org/) [4]. Diabetes mellitus is a chronic metabolic disorder characterized by persistent hyperglycemia caused by absolute or relative deficiency of insulin, depending on the type of diabetes [5]. Prolonged delivery of insulin could significantly contribute to advancement of the pharmaceutical technology currently in use for management of diabetes, particularly, if exploited for delivery of long-acting insulin analogs (*e.g.,* insulin glargine).

Among the physicochemical properties of nanoparticles, particle shape has a profound influence on their interaction with biological systems, including cellular binding and internalization, blood circulation time, bio-distribution, endocytosis by immune cells, and residence time within the cell [6–9]. However, elucidating the effect of nanoparticle shape on cellular binding and uptake is somewhat controversial [10,11]. Some studies have reported notable internalization for spherical shapes compared to non-spherical constructs [10,12]. On the contrary, other studies have reported efficient cellular internalization of rod, discoid, cylinder, triangle sharp-shaped, and quasi-ellipsoidal nanoparticles compared to spherical particles [13,14]. Gratton et al. reported high internalization rates of rod-like, high-aspect-ratio hydrogel particles with dimensions as large as 3 μm by human cervical carcinoma epithelial (HeLa) cells compared with spheres, cylinders, and cubes [15]. Banerjee et al. demonstrated a 2-fold higher internalization capacity of rod-shaped nanoparticles compared to spherical nanoconstructs [16]. Liu et al. revealed the effect of aspect ratio of rod-like nanoparticles on cellular uptake, showing that rods with aspect ratios of 4 and 8 were ingested much faster by both epithelial and endothelial cells than rods with an aspect ratio of 17 [17]. Torpedo-shaped nanocapsules with an aspect ratio of 2.4 exhibited rapid cellular uptake and accumulation compared to their spherical analogues [18]. These observations illustrate that the concept of "one size or shape fits all" does not apply and emphasize the pivotal role of nanoparticle morphology and dimension (shape and aspect ratio) in creating optimized therapeutic carriers.

In our recent work, we have synthesized multifunctional polymer nanocarriers of tunable size and morphology *via* crystallization-driven self-assembly (CDSA) to afford formation of spheres, cylinders, and platelets [19,20]. These nanoparticles were assembled from amphiphilic block copolymers of zwitterionic poly(D-glucose carbonate) and semicrystalline poly(L-lactide) segments, and loaded with silver cation antimicrobials to enhance uroepithelial cell binding. The elongated cylindrical and platelet nanoconstructs exhibited enhanced uroepithelial binding with significant internalization in the case of platelet nanoparticles. The synthesized nanoparticles exhibited negligible cytotoxicity, immunotoxicity, and cytokine adsorption, confirming the biocompatibility of zwitterionic assemblies, while also offering silver cation loading capacity, sustained release, and *in vitro* antimicrobial activity against two *Escherichia coli* strains. Inspired by the substantial impact of nanoparticle shape, here, we report an evaluation of the effect of nanoparticle morphology and dimension on *in vitro* cellular internalization and *in vivo* pharmacological activities of short- and long-acting insulin peptides. Nanoparticles of diverse morphologies were able to prolong the hypoglycemic activity of both types of peptides (insulin and insulin glargine), compared to the free peptides. Spherical and cylindrical nanoparticles demonstrated statistically significant differences in the relative pharmacological availabilities compared to the administration of free insulin, whereas only cylinidrical nanoparticles resulted in statistically significant difference after *in vivo* administration, compared to the free insulin glargine.

2. Materials and methods

2.1. Materials

Nanopure water (18.2 MΩ·cm) was acquired through a Milli-Q water filtration system from Millipore Corp (Burlington, MA). Insulin and insulin glargine (Lantus®) were obtained from Novo Nordisk Limited and Sanofi-aventis US LLC., respectively. Vascular smooth muscle cells were kindly gifted by Dr. Andrea Trache at Texas A&M Health Science Center. Dulbecco's Modified Eagle's Medium (DMEM/F12) was obtained from Life Technologies (Carlsbad, CA), while media additives (fetal bovine serum, HEPES, penicillin/streptomycin) were purchased from Sigma-Aldrich (St. Louis, MO). Cell culture 96-well round-bottom plates were purchased from Corning Costar Co. (Corning, NY). All other chemicals were purchased from Sigma-Aldrich (St. Louis, MO) and used without further purification, unless otherwise noted.

2.2. Synthesis of multifunctional amphiphilic copolymers of varied morphology

Diblock copolymers were synthesized as reported in our previous studies [19,20]. Briefly, diblock copolymers were synthesized through sequential ring-opening polymerizations (ROPs) of alkyne-functionalized cyclic D-glucose carbonate, followed by L-lactide. In a one-pot sequential ROP process, the cyclic carbonate of glucose was allowed to undergo polymerization at −78 °C in dichloromethane for 10 min, followed by removal of the reaction mixture from the dry ice/acetone bath and the introduction of L-lactide and additional dichloromethane, with the polymerization being allowed to proceed for an additional 2–3 min before being quenched by addition of acetic acid. The polymers were then modified *via* photo-initiated thiol-yne click reaction with cysteine (10 equivalents to alkyne groups) under UV light (365 nm) in the presence of 2,2-dimethoxy-2-phenylacetophenone (DMPA) for 2 h, to facilitate quantitative conversion of the alkyne functional groups, render the poly(D-glucose carbonate) segment zwitterionic, and afford the final multi-functional di*block* copolymer poly(D-glucose carbonate)(cysteine)-*block*-poly(L-lactide) [PDGC(cys)-*b*-PLLA].

2.3. Preparation and characterization of insulin- and insulin glargine-loaded nanoparticles

The functional and degradable diblock copolymer PDGC(cys)-*b*-PLLA was assembled into nanocarriers of various sizes and morphologies, and loaded with insulin and insulin glargine. Nanoparticles were assembled following our published protocol [19]. PDGC(cys)-*b*-PLLA was dissolved in nanopure water at concentrations between 0.05 and 0.1 mg/mL and stirred overnight at room temperature. The solutions were then heated to 65 °C for 30 h to aid dissolution, and then removed from heat and allowed to cool to room temperature. Freshly prepared (1) unloaded, (2) insulin-loaded, and (3) insulin glargine-loaded nanoparticles were analyzed for particle size and particle size distribution (polydispersity index, PDI) *via* dynamic light scattering (DLS, Zetasizer Nano ZS, Malvern Instruments, Worcestershire, UK), equipped with a backscattered light detector operating at 173°. Zeta potential values (mV) were measured by laser Doppler anemometry using a Malvern Zetasizer Nano series ZS instrument. Measurements were performed in triplicates at 25 °C.

2.4. Morphological evaluation of nanoparticles

Morphology of nanoparticles was examined using transmission electron microscopy (TEM). TEM images were collected on a JEOL 1200EX operating at 100 kV, and micrographs were recorded at calibrated magnifications using an SIA-15C CCD camera. The samples as aqueous solutions (8 μL) were deposited onto carbon-coated copper grids. Excess sample was wicked off using a filter paper, and the grids

were allowed to dry under ambient conditions. Where indicated, grids were stained with 8 μL of a 1% phosphotungstic acid aqueous solution. After 30 s, excess stain solution was quickly wicked off using a piece of filter paper, and the samples were left to dry under ambient conditions prior to imaging.

2.5. Gel retardation assay

Gel electrophoresis was carried out to examine the binding of insulin (3.5, 7, 14 and 28 *w/w* %) to nanoparticles of different morphologies. FITC-labeled insulin-loaded nanoparticles at a concentration of 0.1 mg/mL for spherical and cylindrical nanoparticles and 0.05 mg/mL for the platelet-like nanoparticles were added in each well (volume *per* well = 50 μL) and was run on 1.5% agarose gel. FITC-labeled insulin was used as a control. Gel electrophoresis was carried out using a horizontal apparatus at 40 V for 75 min, and fluorescence imaging of the FITC-insulin bands was performed using a ChemiDoc XRS imager and the data were analyzed using Image Lab software (Bio-Rad Laboratories, Inc., Hercules, CA).

2.6. Biocompatibility and cellular uptake studies

Three-dimensional (3D) spheroids were cultured and used to investigate the biocompatibility and cellular trafficking of the insulin-loaded zwitterionic nanoparticles. Vascular smooth muscle cells (SMCs) were isolated from rat cremaster arterioles and were cultured in 5% CO_2 at 37 °C in DMEM/F12 supplemented with 10% fetal bovine serum, 10 mM HEPES, 2 mM L-glutamine, 1 mM sodium pyruvate, 100 U/mL penicillin, 100 mg/mL streptomycin and 0.25 mg/mL amphotericin B. Smooth muscle cells were seeded in a round-bottom, ultra-low attachment spheroid microplates at a density of 10,000 cells *per* well in 100 μL of DMEM/F-12 media. Fibroblasts (FBs, 3 T3 embryonic mouse cells) were seeded in a similar way but in media composed of DMEM, 10% FBS and 1% penicillin-streptomycin antibiotics. Spheroids were formed after incubation at 37 °C, 5% CO_2, for 36 h. Afterwards, 50 μL of each formulation was added to the wells. For biocompatibility experiments, insulin-loaded nanoparticles were utilized, whereas for intracellular trafficking purposes, FITC-insulin-loaded nanoparticles were used. Each formulation was prepared from 1 mL of 0.05 mg/mL of each type of the nanoparticles (spherical, cylindrical or platelets) and 5 μL of FITC-insulin (20 U/mL, Sigma Aldrich) or 1 μL of insulin (100 U/mL). Control was prepared from 1 mL of water and 5 μL of FITC-insulin (20 U/mL) or 1 μL of insulin (100 U/mL).

The 3D spheroids were imaged at 5 and 24 h following addition of the formulations. Spheroids were stained with LIVE/DEAD® stain (50 μL) (calcein-AM with ethidium homodimer-1) *per* manufacturer instructions. To image the LIVE/DEAD stained spheroids, laser wavelengths of 488 nm (calcein-AM "live" stain), 543 nm (ethidium homodimer-1 "dead" stain), and 635 nm (transmitted light) were used along in-depth scanning mode (step size = 10 μm). For cellular trafficking, cells were stained with NucRed™ Live 647 ReadyProbes™ Reagent (50 μL), and imaged using laser wavelengths of 488 nm (FITC), 647 nm (NucRed™ stain), and 635 nm (transmitted light) along in-depth scanning mode (step size = 10 μm). Maximum intensity z-stack projections of the fluorescent images were then overlaid on their corresponding transmitted light images. The spheroids were imaged on a laser scanning confocal microscope (FV-1000, Olympus Co.) and images were analyzed in ImageJ (NIH, v. 1.50i).

2.7. In vivo evaluation of hypoglycemic activities of insulin and insulin glargine-loaded nanoparticles

This study was approved by the institutional Animal Ethical Committee of Assiut University, and it adheres to the *Guide for the Care and Use of laboratory Animals,* 8th Edition, National Academies Press, Washington, DC. Wistar rats of either sex and an average body weight of *ca.* 200 g were used to study the pharmacological effects of the prepared insulin/insulin glargine-loaded nanoparticles compared to unloaded insulin/insulin glargine administered as controls. After two weeks of acclimatization in the Animal House, diabetes was induced in rats *via* intraperitoneal administration of 1 mL of alloxan monohydrate solution prepared in phosphate buffered-saline at 60 mg/kg, as previously described [21,22]. After alloxan administration, the blood glucose levels of the rats were monitored using a glucometer (Accu-Check, Roche, USA) until the diabetic state was reached (*i.e.*, persistent blood glucose levels above 200 mg/dL along with signs of diabetes were considered diabetic). Control groups received insulin or insulin glargine while test groups received a subcutaneous injection (1 mL) of tested nanoparticles (7% insulin loading) at a dosage of 0.5 U/kg: Group I was injected subcutaneously with insulin (0.5 U/kg), Groups II, III & IV were subcutaneously injected with insulin-loaded spherical, cylindrical, and platelet-like nanoparticles, respectively, Group V was injected subcutaneously with insulin glargine (0.5 U/kg), and Groups VI, VII, VIII were subcutaneously injected with insulin glargine-loaded spherical, cylindrical, and platelet-like nanoparticles, respectively. One drop of blood was withdrawn from the tail veins of rats before the experiments and at different time intervals following the administration of insulin. The blood glucose levels of rats after administration of insulin/insulin glargine that were either free or loaded into zwitterionic nanoparticles of different morphologies were measured using Freestyle Freedom Lite Glucose Meter (Abbott, East Lansing, MI), and the areas above the blood glucose level time curves (AACs) were calculated by the trapezoidal method [23]. The relative pharmacological availabilities of the insulin/insulin glargine loaded into the nanoparticles were calculated by comparing the AAC following subcutaneous administration to that of free insulin and insulin glargine, as described previously with slight modifications [24]. For consistency, AACs were measured for short- and long-acting insulin that were either free or loaded into nanoparticles, for constant durations of 48 h and 72 h, respectively. Some of the tested samples resulted in a return to the initial blood glucose level before the entire AAC duration (*i.e.,* 48 or 72 h), and it was unethical to continue measuring blood glucose levels after they returned close to the initial levels. Hence, in those cases, we halted taking measurements and assumed that the blood glucose level would remain at the initial value until the end of the experiments. Values are presented as means ± SDs of at least five independent experiments. Significant differences between groups were evaluated by one-way ANOVA followed by Tukey's multiple comparison tests. Differences between different groups were considered significant for p values less than 0.05.

3. Results and discussion

3.1. Preparation and characterizations of insulin-loaded nanoparticles

Multifunctional, fully degradable synthetic zwitterionic block copolymers of PDGC(cys)-*b*-PLLA of varying block lengths were designed to afford micellar nanostructures of spherical, cylindrical, and platelet-like morphologies based on the weight percentage of PLLA in the copolymers [19]. Copolymers with the lowest PLLA content yielded spherical micelles, due to the strong repulsion between the hydrophilic PDGC-cys chains of polymers, which favored the formation of spherical structures with high interfacial curvature upon aqueous CDSA. On the contrary, cylindrical and platelet-like nanostructures were formed upon increasing PLLA weight percentage and this was attributed to the insufficient coronal repulsion in case of high hydrophobic content. Sun et al. showed that for PLLA-*b*-poly(acrylic acid) copolymers, higher hydrophobic weight fraction led to formation of lamellar particles with low interfacial curvature because of insufficient corona repulsion, while spherical structures were formed when polymers of lower hydrophobic fractions were used [25]. Furthermore, Hurst et al. reported that longer PLLA in PLLA-*b*-PEG copolymers resulted in formation of lower corona density and facilitated the formation of 3D structures [26].

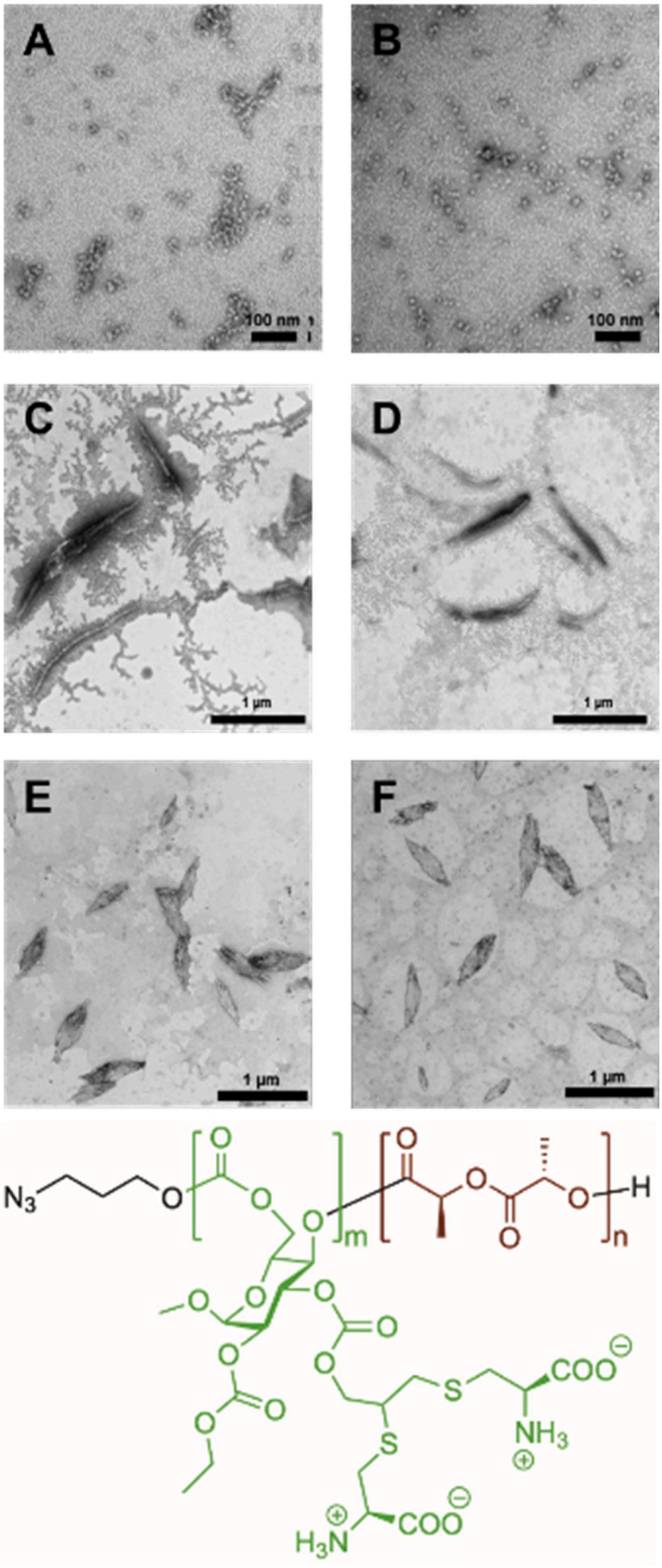

Fig. 1. Transmission electron microscopy images of A) insulin-loaded spherical NPs, B) insulin glargine-loaded spherical NPs, C) insulin-loaded cylindrical NPs, D) insulin glargine-loaded cylindrical NPs, E) insulin-loaded platelet NPs, and F) insulin glargine-loaded platelet NPs at 7% *w/w* loading. The fundamental chemical structure of the polymers having different block segment degrees of polymerization to afford the formation of spherical (m = 70, *n* = 18), cylindrical (m = 47, *n* = 44) and platelet (m = 39, *n* = 74) morphologies upon multi-molecular supramolecular assembly in water, are also indicated. Schematic illustrations of the diverse morphological nanostructures are provided in ref. 19.

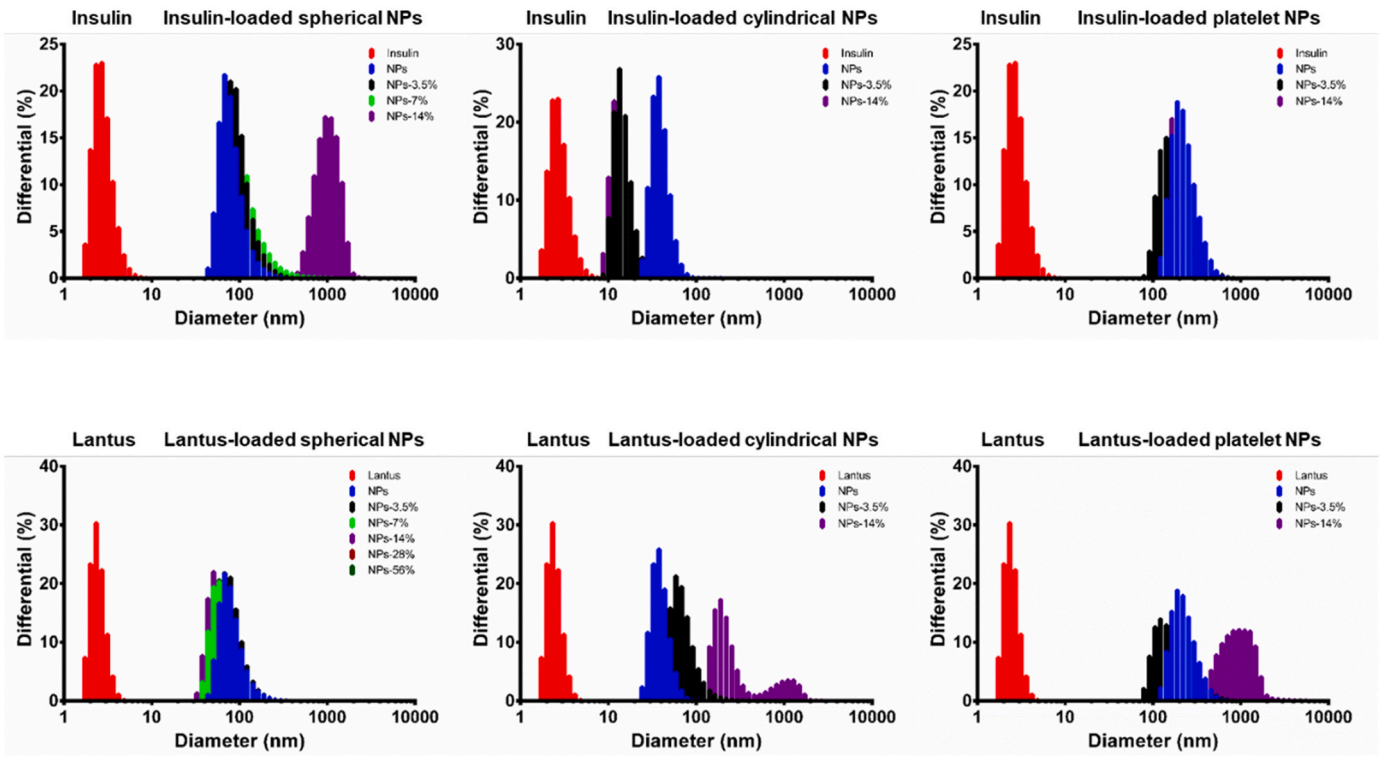

Fig. 2. Histograms of the number-averaged hydrodynamic diameters for overlaid data that were collected from separately prepared and measured samples that include insulin or insulin glargine (Lantus) as free peptides *vs.* peptides added to solutions of zwitterionic polymer nanoparticles of diverse morphologies (spherical, cylindrical and platelet), loaded with varying amounts of insulin and insulin glargine as indicated by the %*w/w* values. Each distinctly colored histogram was collected for a different sample formulation.

The nanoparticles were mixed with insulin and insulin glargine at various loading ratios. Insulin and insulin glargine that were either free or loaded into nanoparticles were characterized in terms of size, size distribution, zeta potential, morphology, and insulin binding affinity. Encapsulation of insulin and insulin glargine into zwitterionic nanoparticles could occur *via* various mechanisms, for instance, through interactions with the amino groups within the hydrophilic nanostructure corona. TEM studies indicated that spherical, cylindrical and platelet-like morphologies of PDGC(cys)-*b*-PLLA nanoparticles were retained after loading of insulin and insulin glargine (Fig. 1). Cluster formation was observed only for insulin-loaded spherical polymer nanoparticles (Supplementary Materials, Fig. S1). This phenomenon might be due to lower surface charge of insulin (isoelectric point = 5.3) at the acidic pH value of the nanopure water, and possibility of interactions between insulin molecules and more than one spherical nanoparticle simultaneously. This phenomenon of cluster formation was not observed with insulin glargine (isoelectric point = 6.7), probably due to the higher charge density at the pH of the solution (*ca.* 5.5). Cluster formation was also not observed with cylindrical and platelet nanoparticles, possibly due to the lower collision incidence compared to their spherical counterparts. Aside from technical complications that were experienced from the cluster formation between insulin and spherical nanoparticles, the particle-particle aggregation provides evidence for the association of peptides with the synthetic nanocarriers.

Histograms of the intensity-, volume-, and number-averaged hydrodynamic diameters of insulin, insulin glargine, zwitterionic polymer nanoparticles of diverse morphologies (spherical, cylindrical and platelet), unloaded and loaded with varying amounts of insulin and insulin glargine were generated to allow for further investigation of the peptide-nanoparticle interactions (Fig. 2). The histograms illustrate efficient binding of peptides (*i.e.* insulin and insulin glargine) to nanoparticles, as evidenced by the absence of free insulin peaks (*ca.* 2–5 nm) in the insulin-loaded nanoparticle histograms. Detailed information on

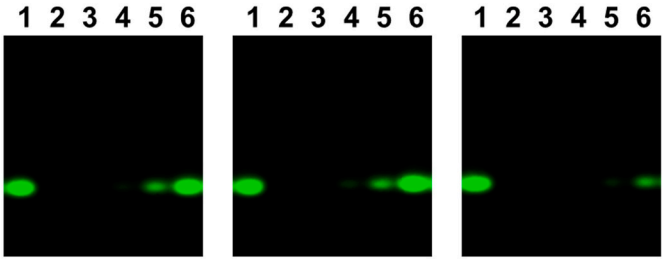

Fig. 3. Gel retardation assay of FITC-insulin that is either free (lane 1) or loaded at 3.5 (lane 3), 7 (lane 4), 14 (lane 5), and 28%*w/w* (lane 6), into spherical (left panel), cylindrical (middle panel) and platelet-like nanoparticles (right panel) onto agarose gel at 40 V for 75 min. Unloaded nanoparticles are also shown on the respective gel (lane 2). Agarose gels were prepared at 1.5%, nanoparticles were prepared at concentrations of 0.1 mg/mL for spherical and cylindrical nanoparticles, and at 0.05 mg/mL for platelet nanoparticles (volume *per* well = 50 μL).

sizes, size distributions and zeta potentials of insulin/insulin-glargine-loaded nanoparticles of diverse morphologies are also available (Supplementary Materials, Tables S1-S6). It is worth mentioning that the zwitterionic character of the nanoparticles may exist only within a specific pH range, over which the charged groups have intra salt structures and become electrically neutral. Experiments were, therefore, conducted in nanopure water at pH 5.5. Nonetheless, along the polymer backbone and between polymer chains in nanoscopic assemblies, there may also be intra- and/or intermolecular polymer side chain interactions that either do not allow the expected protonation of amine groups or may lead to the inadvertent protonation of carboxylates in this pH range. The zeta potential values were generally negative for the nanostructures, suggesting either negative or neutral states for the side chain moieties, and they became less negative upon binding positively-

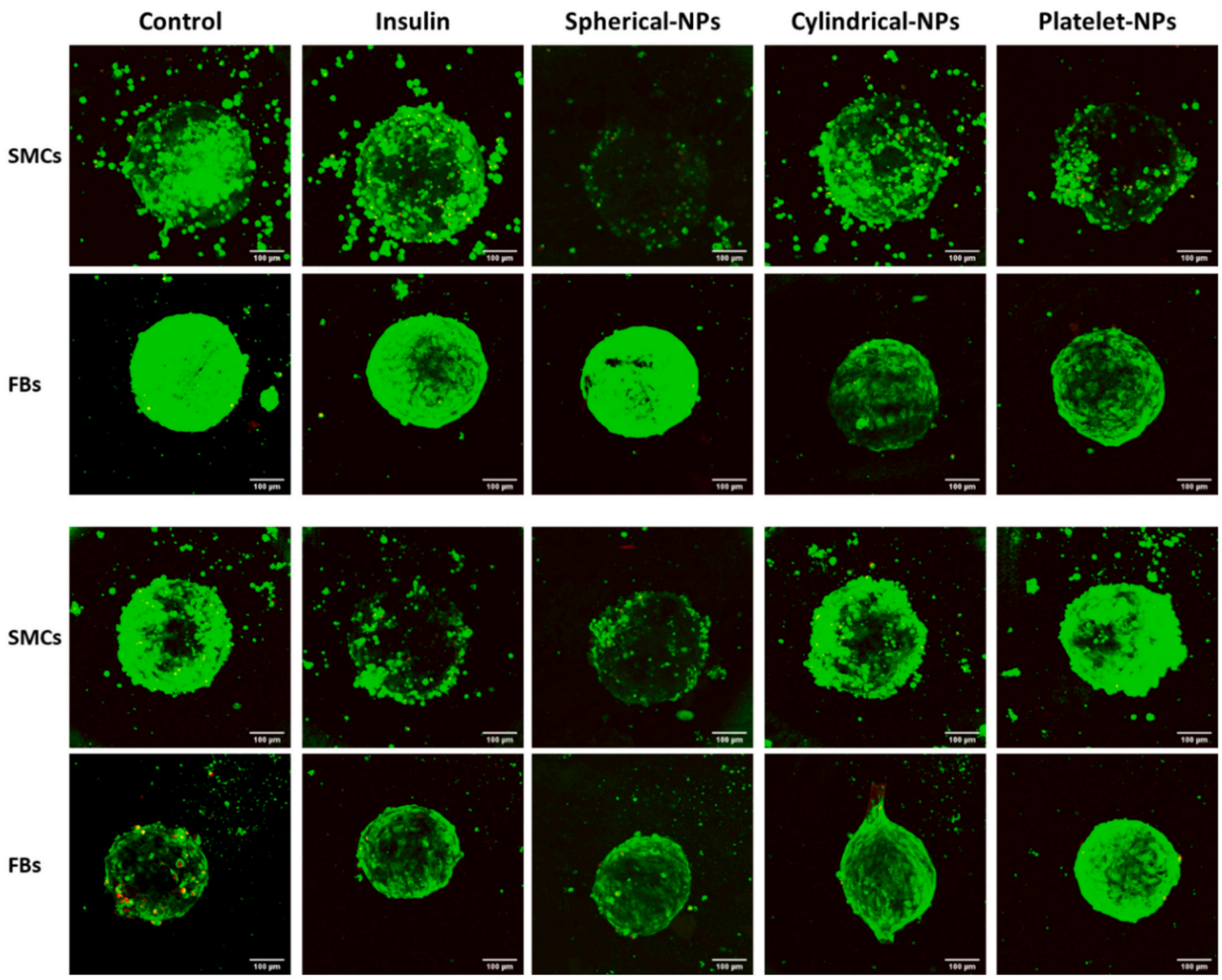

Fig. 4. Laser scanning confocal microscopy images of 3D spheroids of SMCs and FBs that were either untreated (control) or treated with insulin, insulin-loaded nanoparticles of spherical, cylindrical and platelet morphologies for 5 h (upper panel) and 24 h (lower panel). Cells were then treated with LIVE/DEAD® stain (calcein-AM and ethidium homodimer-1). Laser wavelengths of 488 nm (calcein-AM "live" stain) and 543 nm (ethidium homodimer-1 "dead" stain) were used along in-depth scanning mode (step size = 10 μm). Maximum intensity z-stack projections of the fluorescent images were then overlain on their corresponding transmitted light images. The presented scale bars measure 100 μm.

charged insulin glargine, Lantus. Binding of insulin by the nanoparticles was further confirmed by gel retardation assays (Fig. 3). For this purpose, FITC-labeled insulin was utilized to spike the insulin-loaded nanoparticles that were loaded onto agarose gel and the gel migrations were compared against the free FITC-labeled insulin, as a control. Unloaded insulin migrated freely, whereas nanoparticle-loaded insulin could not migrate through the gel, as indicated by the absence of insulin bands within the agarose gel, at insulin loading of 3.5 and 7%*w/w*. However, upon increasing insulin loading, partial migration of insulin occurred. It was obvious that platelet-like nanoparticles had higher binding capacity to insulin, compared to nanoparticles of other morphologies (*i.e.* spherical and cylindrical). Hence, insulin- and insulin glargine-loaded nanoparticles at 7% loading were selected for further studies. Future studies will focus on studying the effect of pH on morphology of the assemblies and the binding/release behavior.

3.2. Biocompatibility of insulin-loaded nanoparticles

To assess biocompatibility of insulin-loaded nanoparticles, spheroids of SMCs and FBs were treated with insulin, and insulin-loaded nanoparticles of spherical, cylindrical and platelet-like morphologies for 5 h (Fig. 4, upper panel) and 24 h (Fig. 4, lower panel). Then, LIVE/DEAD® stain (calcein AM and ethidium homodimer-1) was added to cells to identify living cells based on their ability to convert calcein AM (which is easily diffused through living cells) by intracellular esterase enzyme activity to its fluorescent equivalent (green stain). Damaged or dead cells are stained red with ethidium bromide, since only leaky cells allow DNA exposure to ethidium bromide. The results confirmed that insulin-loaded nanoparticles are biocompatible with no signs of toxicity observed in both cell lines, as revealed by the absence of red staining of dead cells after 5 and 24 h of incubation. This can be attributed to biocompatibility and biodegradability of polymers used (*i.e.* aliphatic polycarbonates and PLLA) [27]. Moreover, grafting of biocompatible L-cysteine in the block copolymer, imparted a zwitterionic character to the micelle surface, which is desirable for inhibiting aggregation in physiological milieu and for circumventing toxicity concerns associated with cationic polymers [19,28]. Previous work by our group showed that amphiphilic block copolymers of zwitterionic poly(D-glucose carbonate)

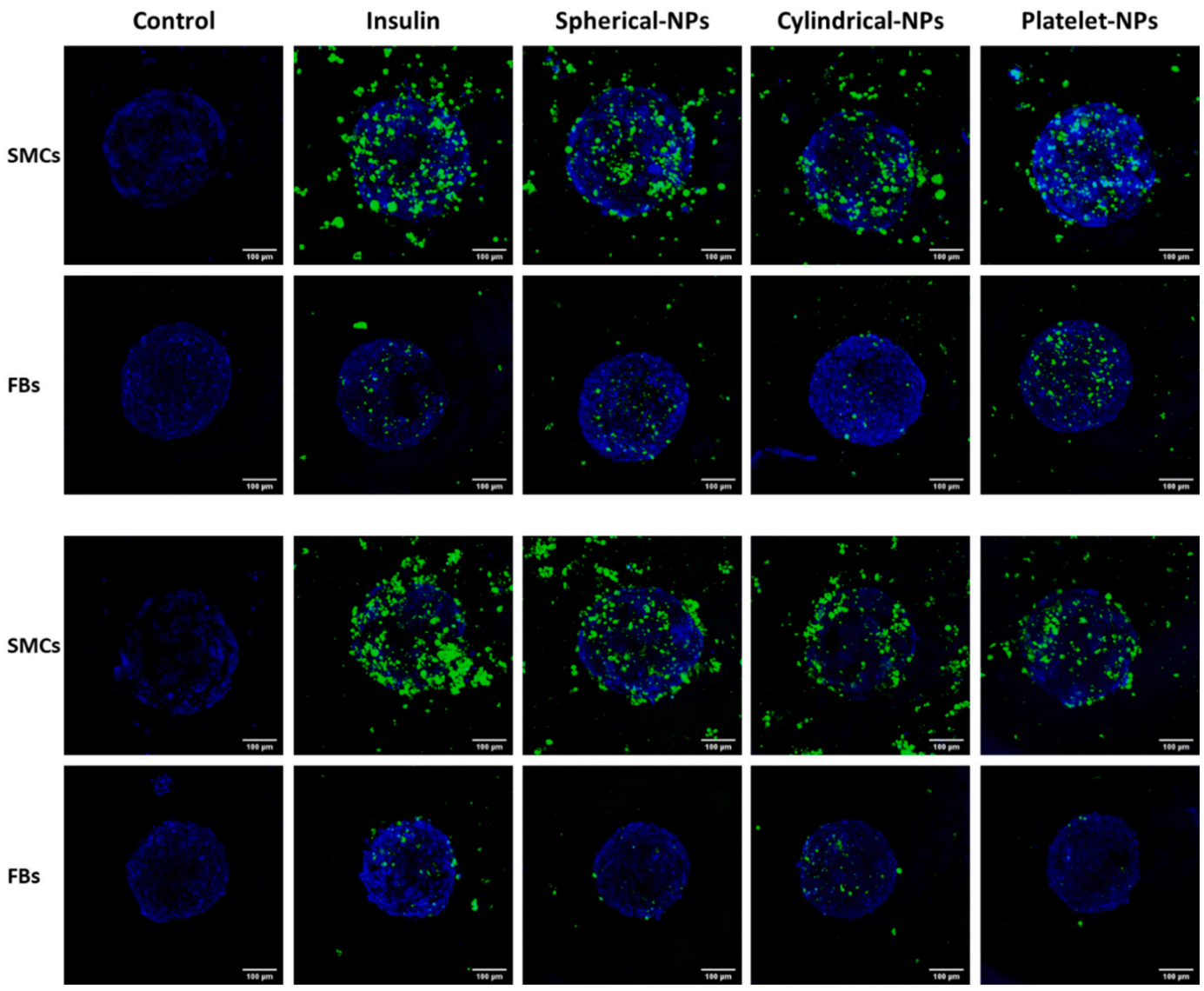

Fig. 5. Laser scanning confocal microscopy images of 3D spheroids of SMCs and FBs that were either untreated (control) or treated with FITC-insulin, FITC-insulin-loaded nanoparticles of spherical, cylindrical and platelet morphologies for 5 h (upper panel) and 24 h (lower panel). Laser wavelengths of 488 nm (FITC) and 647 nm (NucRed™ stain) were used along in-depth scanning mode (step size = 10 μm). Maximum intensity z-stack projections of the fluorescent images were then overlaid on their corresponding transmitted light images. The presented scale bars measure 100 μm.

and semicrystalline poly(L-lactide) segments exhibited negligible cytotoxicity against uroepithelial cells and no significant immunotoxicity was observed in RAW 264.7 macrophages [20]. Finnegan and *co*-workers reported the absence of cytotoxicity in healthy (WI-38) and cancerous HeLa cells upon treatment with a polycarbonate derivative-*b*-PEG copolymer (at a concentration range of 1–100 g/mL) prepared by CDSA [29]. Videos of 3D images are also available (see Supplementary Materials, videos are supplied in a separate Ms. PowerPoint file). The videos clearly demonstrate the viability of both cell lines after their incubation with insulin-loaded nanoparticles of varying morphologies for 5 and 24 h, indicated by the appearance of green fluorescence in live cells and absence of red staining.

3.3. Cellular uptake of FITC-insulin loaded nanoparticles

To gain an insight on cellular uptake of the prepared nanoparticles, intracellular trafficking of FITC-insulin-loaded nanoparticles was investigated by confocal microscopy in SMCs and FBs at 5 h (Fig. 5, upper panel) and 24 h (Fig. 5, lower panel) after incubation with nanoparticles. For SMCs, there was an appreciably high visible cell-associated fluorescence after incubation with either FITC-insulin alone or FITC-insulin loaded nanoparticles indicating a significant uptake of loaded insulin (Fig. 5, and Supplementary Materials: videos are supplied in a separate Ms. PowerPoint file). Resolution on these images is not enough to demonstrate differences between sizes and morphologies of the particles, especially after binding with biomolecules in the cell culture media and to the various cellular components. On the contrary, a weak fluorescent signal appeared in the case of FBs upon their incubation with similar treatments for the same time intervals. These results clearly point out that nanoparticle uptake is not only limited to their size and shape but is also dependent on cell type (*i.e.,* for a given nanoparticle, different internalization capacity can be observed by different cell types). Dos Santos et al., showed that internalization of nanoparticles was dependent on their size and varied in different cell lines, possibly due to different uptake mechanisms and nature of cells [30]. Banerjee et al. also showed differential uptake capacity of spherical nanoparticles prepared at different sizes, with consistently higher uptake in Caco-2/HT-29 cells compared to Caco-2 monolayers [16].

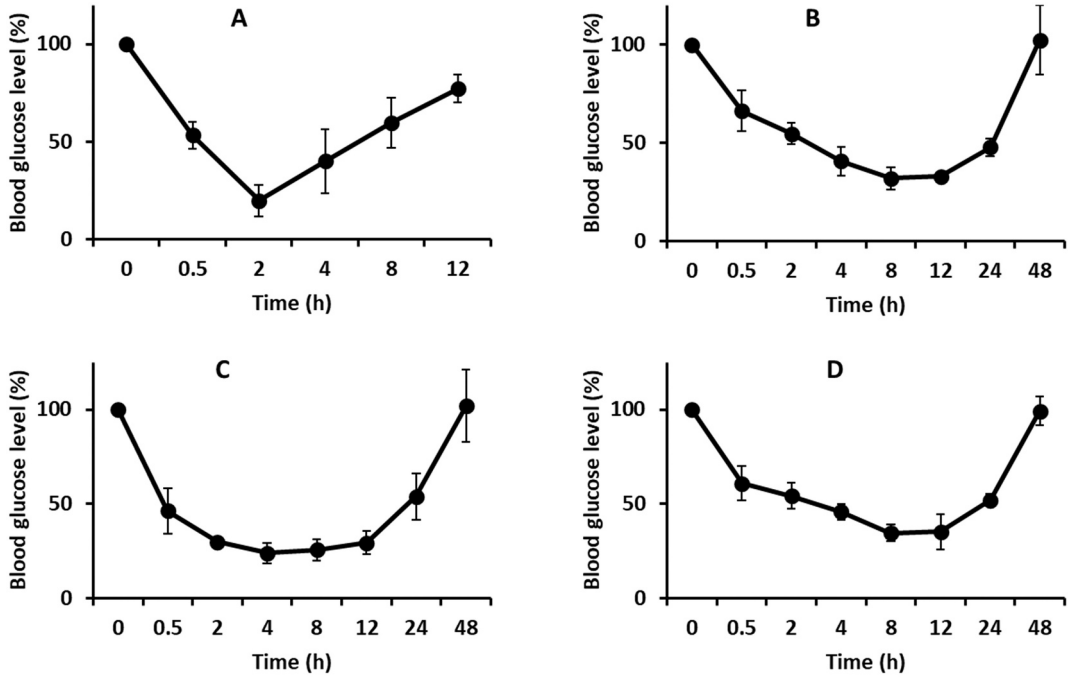

Fig. 6. Blood glucose levels in diabetic rats following subcutaneous injection of insulin (0.5 U/kg) that was either free (A), or loaded into spherical (B), cylindrical (C) and platelet-like (D) nanoparticles (7% *w/w* insulin loading, 1 mL volume for subcutaneous injection).

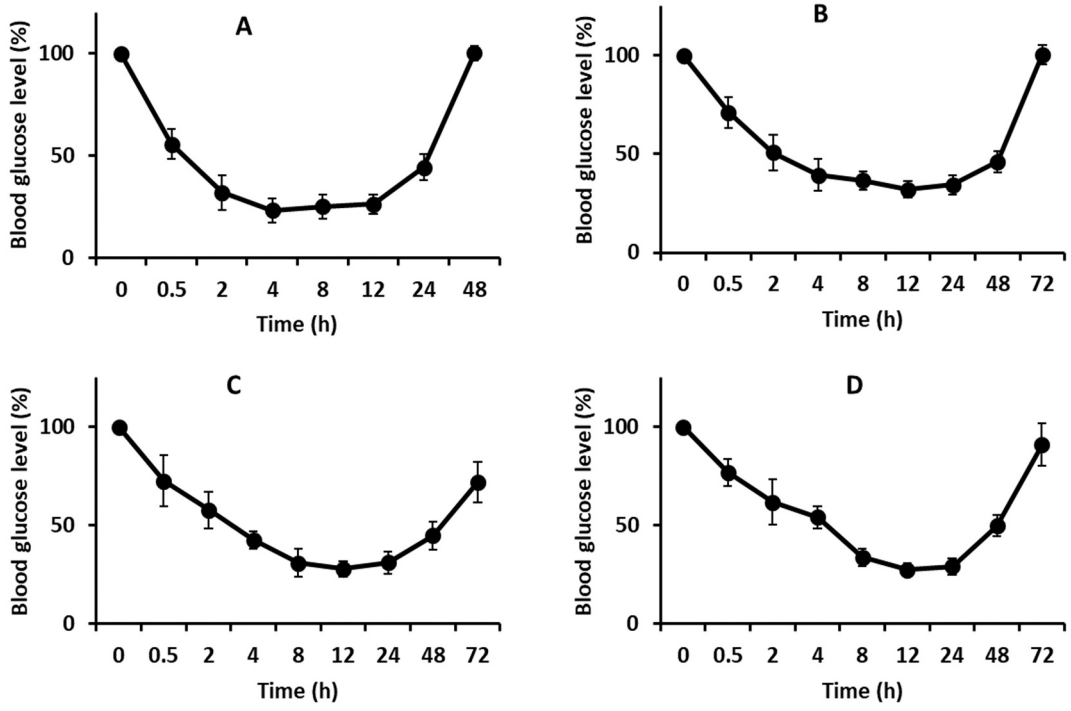

Fig. 7. Blood glucose levels in diabetic rats following subcutaneous injection of insulin glargine (0.5 U/kg) that was either free (A), or loaded into spherical (B), cylindrical (C) and platelet-like (D) nanoparticles (7% *w/w* insulin glargine loading, 1 mL volume for subcutaneous injection).

3.4. In vivo hypoglycemic activities in diabetic rats

Normalization of blood glucose levels in diabetic patients is the main purpose in management of diabetes. In normal individuals, endogenous insulin is maintained at low basal plasma levels in fasting state and increases upon meal intake. In diabetic patients, insulin production is insufficient, or the body does not respond appropriately to insulin. Insulin and insulin glargine are short- and long-acting analogs that usually exhibit maximum hypoglycemic activity at 2 and 12 h after administration and commonly exhibit durations of action of *ca.* 6 h and 24 h, respectively. The standard for medical management of diabetes for many years has included the prescription of human insulin. However, its short *in vivo* half-life results in frequent administration and patient incompliance. Hence, long acting analogs of insulin (*e.g.* insulin glargine) that have prolonged duration of action were developed. Insulin glargine is formed *via* replacing the asparagine at position 21 of the A

chain with glycine in human insulin, and addition of two arginines to the C-terminus of the B chain. Subcutaneous administration of insulin glargine once daily is prescribed for a prolonged blood glucose lowering effect (*ca* 24 h) compared to insulin [31–33].

To investigate the efficiency of fabricated nanoparticles in prolonging the antidiabetic effect of insulin and insulin glargine, diabetic rats were subcutaneously injected with insulin/insulin-glargine that were either free or loaded into nanoparticles of different morphologies, and blood glucose levels were monitored. Subcutaneous injection of insulin (0.5 U/kg) resulted in a significant hypoglycemic effect that was maintained for 2 h, and then blood glucose level recovered to the initial level (Fig. 6A). Subcutaneous administration of insulin-loaded nanoparticles induced a significant sustained hypoglycemic effect and maintained low blood glucose level over 24 h (Fig. 6B-D). Subcutaneous administration of insulin-glargine, a long-acting analog of insulin, showed a sustained hypoglycemic effect over 24 h that was increased to 48 h after incorporation into nanoparticles (Fig. 7A-D).

The relative pharmacological availabilities of insulin and insulin glargine, unloaded or loaded into nanoparticles of various morphologies, were calculated based on the AAC following their subcutaneous administration. Insulin loaded into spherical and cylindrical nanoparticles had demonstrated significantly higher AACs (9300 ± 2700 mg·h/dL and 9200 ± 3700 mg·h/dL, respectively) compared to free insulin (3500 ± 900 mg·h/dL) ($p < 0.05$), whereas insulin-loaded platelet nanoparticles' AAC (7900 ± 2300 mg·h/dL) was not significantly higher than free insulin ($p > 0.05$). Only insulin glargine loaded into cylindrical nanoparticles had shown significantly higher AAC (18,900 ± 3800 mg·h/dL) compared to free insulin glargine (10,900 ± 2500 mg·h/dL) ($p < 0.05$), whereas the AAC values (16,300 ± 4100 mg·h/dL 17,300 ± 4300 mg·h/dL, respectively) for insulin glargine-loaded spherical and platelet nanoparticles, respectively, were not significantly higher than free insulin glargine ($p > 0.05$). It can be clearly seen that loading of insulin and insulin glargine into nanoparticles of diverse morphologies had resulted in 2.3–2.6-fold and 1.5–1.7-fold higher AAC compared to free insulin and insulin glargine, respectively, and thus, led to a significant improvement in the pharmacological availability, extension of the hypoglycemic activity, reduction in frequency of administration, and overall improvement in patient compliance.

Nanoparticles have been reported previously to extend hypoglycemic activity of insulin after subcutaneous administration [34–36]. However, studies available on the effect of nanoparticles on prolonging hypoglycemic activity of insulin glargine following subcutaneous administration in the literature are scarce. The results demonstrated in the current study provide evidence that nanoparticles of varying morphologies efficiently interacted with insulin and insulin glargine and allowed extended hypoglycemic activities. It is uncertain, at the moment, to what extent such an extended biological activity is due to stabilization of primary and/or secondary structure, extended subcutaneous retention and duration of release, or other effects. However, construction of these types of biodegradable and biocompatible assemblies might provide clinically-viable formulations for enhanced future management of diabetes. Furthermore, control of morphology of the formed assemblies together with possibility of covalently attaching peptides or other biomolecules onto the nanoparticles may provide for additional optimization toward prolonged hypoglycemic activity. Future experiments may also elucidate the role of nanoparticles in stabilizing primary/secondary structures of insulin and insulin glargine, and how it is associated with extending the pharmacological activities of the loaded peptides.

4. Conclusions

In summary, zwitterionic polymer nanoparticles loaded with insulin and insulin-glargine were constructed from biocompatible sugar-based polymers to extend their pharmacological activities. Well-defined nanostructures were prepared *via* CDSA to yield spherical, cylindrical, and platelet-like nanoparticles, as confirmed by TEM. Nanoparticles of the diverse morphologies that were loaded with insulin and insulin-glargine had similar sizes and morphologies to their respective nanoparticles before loading. Nanoconstructs demonstrated high biocompatibility and cellular uptake, as illustrated by confocal microscopy studies in two different cells lines, SMCs and FBs. *Co*-formulation of short-acting insulin and the long-acting insulin glargine with the synthetic polymers generated composite nanoparticles, which resulted in extended hypoglycemic activities in diabetic rat models. This work highlights the use of amphiphilic block copolymers of zwitterionic poly(D-glucose carbonate) and semicrystalline poly(L-lactide) segments to produce functional biocompatible nanoconstructs for management of diabetes and indicates the potential application of nanoparticle-mediated drug delivery of various morphologies in addition to spherical structures traditionally described in the design of nanomedicines.

Author contributions

Y.S. synthesized, prepared and characterized nanoparticles, and wrote the manuscript. M.E. and S.K. performed the gel retardation assay, biocompatibility and cellular uptake studies. M.E., N.G.E. and M.A.H. designed and performed *in vivo* studies, and data analysis and contributed to experimental design. M.E. and K.L.W. conceived the project and wrote the manuscript.

CRediT authorship contribution statement

Mahmoud Elsabahy: Conceptualization, Data curation, Methodology, Project administration, Writing - original draft, Writing - review & editing. **Yue Song:** Data curation, Methodology, Writing - original draft, Writing - review & editing. **Noura G. Eissa:** Data curation, Methodology, Writing - original draft, Writing - review & editing. **Sarosh Khan:** Data curation, Methodology, Writing - original draft, Writing - review & editing. **Mostafa A. Hamad:** Methodology, Project administration, Writing - original draft, Writing - review & editing. **Karen L. Wooley:** Conceptualization, Funding acquisition, Project administration, Writing - original draft, Writing - review & editing.

Acknowledgments

This work was supported by the National Science Foundation (CHE-1610311, CHE-2003771, and DMREF-1629094), and the Robert A. Welch Foundation through the W. T. Doherty-Welch Chair in Chemistry (A-0001). Uses of the Texas A&M University Laboratory for Synthetic-Biologic Interactions (LSBI) and the Texas A&M Microscopy and Imaging Center are acknowledged.

Appendix A. Supplementary data

Supplementary data to this article can be found online at https://doi.org/10.1016/j.jconrel.2021.04.006.

References

[1] J.V. Natarajan, C. Nugraha, X.W. Ng, S. Venkatraman, Sustained-release from nanocarriers: a review, J. Control. Release 193 (2014) 122–138, https://doi.org/10.1016/j.jconrel.2014.05.029.
[2] P. Tyagi, S. Pechenov, J. Anand Subramony, Oral peptide delivery: translational challenges due to physiological effects, J. Control. Release 287 (2018) 167–176, https://doi.org/10.1016/j.jconrel.2018.08.032.
[3] W. Chen, B.C. Yung, Z. Qian, X. Chen, Improving long-term subcutaneous drug delivery by regulating material-bioenvironment interaction, Adv. Drug Deliv. Rev. 127 (2018) 20–34, https://doi.org/10.1016/j.addr.2018.01.016.
[4] M. Laakso, Biomarkers for type 2 diabetes, Mol. Metab. 27 (2019) S139–S146, https://doi.org/10.1016/j.molmet.2019.06.016.
[5] M.N. Piero, G.M. Nzaro, J.M. Njagi, Diabetes mellitus – a devastating metabolic disorder, Asian J. Biomed. Pharm. Sci. 4 (2015) 1–7, https://doi.org/10.15272/ajbps.v4i40.645.

[6] Y. Wang, C. Pi, X. Feng, Y. Hou, L. Zhao, Y. Wei, The influence of nanoparticle properties on oral bioavailability of drugs, Int. J. Nanomedicine 15 (2020) 6295–6310, https://doi.org/10.2147/IJN.S257269.
[7] R. Madathiparambil Visalakshan, L.E. González García, M.R. Benzigar, A. Ghazaryan, J. Simon, A. Mierczynska-Vasilev, T.D. Michl, A. Vinu, V. Mailänder, S. Morsbach, K. Landfester, K. Vasilev, The influence of nanoparticle shape on protein Corona formation, Small. 16 (2020) 2000285, https://doi.org/10.1002/smll.202000285.
[8] J.L. Perry, K.P. Herlihy, M.E. Napier, J.M. Desimone, PRINT: a novel platform toward shape and size specific nanoparticle theranostics, Acc. Chem. Res. 44 (2011) 990–998, https://doi.org/10.1021/ar2000315.
[9] R.A. Petros, J.M. DeSimone, Strategies in the design of nanoparticles for therapeutic applications, Nat. Rev. Drug Discov. 9 (2010) 615–627, https://doi.org/10.1038/nrd2591.
[10] R. Zein, W. Sharrouf, K. Selting, Physical properties of nanoparticles that result in improved cancer targeting, J. Oncol. 2020 (2020) 5194780, https://doi.org/10.1155/2020/5194780.
[11] P. Foroozandeh, A.A. Aziz, Insight into cellular uptake and intracellular trafficking of nanoparticles, Nanoscale Res. Lett. 13 (2018) 339, https://doi.org/10.1186/s11671-018-2728-6.
[12] Y.J. Lee, E.Y. Ahn, Y. Park, Shape-dependent cytotoxicity and cellular uptake of gold nanoparticles synthesized using green tea extract, Nanoscale Res. Lett. 14 (2019) 1–14, https://doi.org/10.1186/s11671-019-2967-1.
[13] R. Augustine, A. Hasan, R. Primavera, R.J. Wilson, A.S. Thakor, B.D. Kevadiya, Cellular uptake and retention of nanoparticles: insights on particle properties and interaction with cellular components, Mater. Today Commun. 25 (2020) 101692, https://doi.org/10.1016/j.mtcomm.2020.101692.
[14] B.D. Kevadiya, B. Ottemann, I.Z. Mukadam, L. Castellanos, K. Sikora, J.R. Hilaire, J. Machhi, J. Herskovitz, D. Soni, M. Hasan, W. Zhang, S. Anandakumar, J. Garrison, J.E. McMillan, B. Edagwa, R.L. Mosley, R.W. Vachet, H.E. Gendelman, Rod-shape theranostic nanoparticles facilitate antiretroviral drug biodistribution and activity in human immunodeficiency virus susceptible cells and tissues, Theranostics. 10 (2020) 630–656, https://doi.org/10.7150/thno.39847.
[15] S.E.A. Gratton, P.A. Ropp, P.D. Pohlhaus, J.C. Luft, V.J. Madden, M.E. Napier, J. M. DeSimone, The effect of particle design on cellular internalization pathways, Proc. Natl. Acad. Sci. U. S. A. 105 (2008) 11613–11618, https://doi.org/10.1073/pnas.0801763105.
[16] A. Banerjee, J. Qi, R. Gogoi, J. Wong, S. Mitragotri, Role of nanoparticle size, shape and surface chemistry in oral drug delivery, J. Control. Release 238 (2016) 176–185, https://doi.org/10.1016/j.jconrel.2016.07.051.
[17] X. Liu, F. Wu, Y. Tian, M. Wu, Q. Zhou, S. Jiang, Z. Niu, Size dependent cellular uptake of rod-like bionanoparticles with different aspect ratios, Sci. Rep. 6 (2016) 2–11, https://doi.org/10.1038/srep24567.
[18] M. Ueda, S. Seo, B.G. Nair, S. Müller, E. Takahashi, T. Arai, T. Iyoda, S.I. Fujii, S. Tsuneda, Y. Ito, End-sealed high aspect ratio hollow nanotubes encapsulating an anticancer drug: torpedo-shaped peptidic nanocapsules, ACS Nano 13 (2019) 305–312, https://doi.org/10.1021/acsnano.8b06189.
[19] Y. Song, Y. Chen, L. Su, R. Li, R.A. Letteri, K.L. Wooley, Crystallization-driven assembly of fully degradable, natural product-based poly(L-lactide)-block-poly(α-D-glucose carbonate)s in aqueous solution, Polymer. 122 (2017) 270–279, https://doi.org/10.1016/j.polymer.2017.06.065.
[20] Y. Song, M. Elsabahy, C.A. Collins, S. Khan, R. Li, T.N. Hreha, Y. Shen, Y.-N. Lin, R. A. Letteri, L. Su, M. Dong, F. Zhang, D.A. Hunstad, K.L. Wooley, Morphologic design of silver-bearing sugar-based polymer nanoparticles for uroepithelial cell binding and antimicrobial delivery, Nano Lett. (2021) *(submitted)*.
[21] M. Gulfraz, G. Qadir, F. Nosheen, Z. Parveen, Antihyperglycemic effects of Berberis lyceum royle in alloxan induced diabetic rats, Prelim. Commun. 36 (2007) 49–54.
[22] A. Lukačínová, J. Mojžiš, R. Beňačka, J. Keller, T. Maguth, P. Kurila, L. Vaško, O. Rácz, F. Ništiar, Preventive effects of flavonoids on alloxan-induced diabetes mellitus in rats, Acta Vet. Brno 77 (2008) 175–182, https://doi.org/10.2754/avb200877020175.
[23] Q. Zhang, Z. Shen, T. Nagai, Prolonged hypoglycemic effect of insulin-loaded polybutylcyanoacrylate nanoparticles after pulmonary administration to normal rats, Int. J. Pharm. 218 (2001) 75–80, https://doi.org/10.1016/S0378-5173(01)00614-7.
[24] C. Liu, Y. Kou, X. Zhang, W. Dong, H. Cheng, S. Mao, Enhanced oral insulin delivery via surface hydrophilic modification of chitosan copolymer based self-assembly polyelectrolyte nanocomplex, Int. J. Pharm. 554 (2019) 36–47, https://doi.org/10.1016/j.ijpharm.2018.10.068.
[25] L. Sun, N. Petzetakis, A. Pitto-barry, T.L. Schiller, N. Kirby, D.J. Keddie, B.J. Boyd, R.K.O. Reilly, A.P. Dove, Tuning the size of cylindrical micelles from poly, Macromolecules. 22 (2013) 9074–9082.
[26] P.J. Hurst, A.M. Rakowski, J.P. Patterson, Ring-opening polymerization-induced crystallization-driven self-assembly of poly-L-lactide-block-polyethylene glycol block copolymers (ROPI-CDSA), Nat. Commun. 11 (2020) 1–12, https://doi.org/10.1038/s41467-020-18460-2.
[27] S. Ganda, M.H. Stenzel, Concepts, fabrication methods and applications of living crystallization-driven self-assembly of block copolymers, Prog. Polym. Sci. 101 (2020) 101195, https://doi.org/10.1016/j.progpolymsci.2019.101195.
[28] R. Shevate, M. Kumar, M. Karunakaran, M.N. Hedhili, K.V. Peinemann, Polydopamine/cysteine surface modified isoporous membranes with self-cleaning properties, J. Membr. Sci. 529 (2017) 185–194, https://doi.org/10.1016/j.memsci.2017.01.058.
[29] J.R. Finnegan, X. He, S.T.G. Street, J.D. Garcia-Hernandez, D.W. Hayward, R. L. Harniman, R.M. Richardson, G.R. Whittell, I. Manners, Extending the scope of "living" crystallization-driven self-assembly: well-defined 1D micelles and block comicelles from crystallizable polycarbonate block copolymers, J. Am. Chem. Soc. 140 (2018) 17127–17140, https://doi.org/10.1021/jacs.8b09861.
[30] T. Dos Santos, J. Varela, I. Lynch, A. Salvati, K.A. Dawson, Quantitative assessment of the comparative nanoparticle-uptake efficiency of a range of cell lines, Small. 7 (2011) 3341–3349, https://doi.org/10.1002/smll.201101076.
[31] K. Uehata, T. Anno, K. Hayashida, K. Motoyama, F. Hirayama, N. Ono, J.D. Pipkin, K. Uekama, H. Arima, Effect of sulfobutyl ether-β-cyclodextrin on bioavailability of insulin glargine and blood glucose level after subcutaneous injection to rats, Int. J. Pharm. 419 (2011) 71–76, https://doi.org/10.1016/j.ijpharm.2011.07.018.
[32] K. Uehata, T. Anno, K. Hayashida, T. Higashi, K. Motoyama, F. Hirayama, K. Uekama, H. Arima, Peak-less hypoglycemic effect of insulin glargine by complexation with maltosyl-β-cyclodextrin, Int. J. Pharm. 422 (2012) 33–39, https://doi.org/10.1016/j.ijpharm.2011.10.022.
[33] D. Sharma, J. Singh, Long-term glycemic control and prevention of diabetes complications in vivo using oleic acid-grafted-chitosan-zinc-insulin complexes incorporated in thermosensitive copolymer, J. Control. Release 323 (2020) 161–178, https://doi.org/10.1016/j.jconrel.2020.04.012.
[34] R. Mo, T. Jiang, J. Di, W. Tai, Z. Gu, Emerging micro- and nanotechnology based synthetic approaches for insulin delivery, Chem. Soc. Rev. 43 (2014) 3595–3629, https://doi.org/10.1039/c3cs60436e.
[35] Z. Chai, H. Dong, X. Sun, Y. Fan, Y. Wang, F. Huang, Development of glucose oxidase-immobilized alginate nanoparticles for enhanced glucose-triggered insulin delivery in diabetic mice, Int. J. Biol. Macromol. 159 (2020) 640–647, https://doi.org/10.1016/j.ijbiomac.2020.05.097.
[36] S.S. Saravanan, M.S. Malathi, S.P.S.L. Sesh, S. Selvasubramanian, B. S. Balasubramanian, P.V. Pandiyan, Hydrophilic poly (ethylene glycol) capped poly (lactic-co-glycolic) acid nanoparticles for subcutaneous delivery of insulin in diabetic rats, Int. J. Biol. Macromol. 95 (2017) 1190–1198, https://doi.org/10.1016/j.ijbiomac.2016.11.009.